High and Stable Ionic Conductivity in 2D Nanofluidic Ion Channels between Boron Nitride Layers

Si Qin, Dan Liu, Guang Wang, David Portehault, Christopher J. Garvey, Yury Gogotsi, Weiwei Lei, Ying Chen

High and Stable Ionic Conductivity in 2D Nanofluidic Ion Channels Between Boron Nitride Layers

Si Qin[1], Dan Liu[1], Guang Wang[1], David Portehault[2], Christopher J. Garvey[3], Yury Gogotsi[4], Weiwei Lei[1] and Ying Chen[1]**

[1] Institute for Frontier Materials (IFM), Deakin University, 75 Pigdons Road, Waurn Ponds, Victoria 3216, Australia

[2] Sorbonne Universités, UPMC Université Paris 06, CNRS, Collège de France, Laboratoire de Chimie de la Matière Condensée de Paris (LCMCP), 11 place Marcelin Berthelot, F-75005 Paris, France

[3] Australia Nuclear Science and Technology Organization (ANSTO), Sydney, New South Wales 2232, Australia

[4] A. J. Drexel Nanomaterials Institute and Materials Science and Engineering Department, Drexel University, 3141 Chestnut Street, Philadelphia, PA 19104, United States

ABSTRACT: Achieving a high rate of ionic transport through porous membranes and ionic channels is important in numerous applications ranging from energy storage to water desalination, but still remains a challenge. Herein we show that ions can quickly pass through interlayer spaces in hydrated boron nitride (BN) membranes. Measurements of surface-charge governed ionic currents through BN conduits in a variety of salt solutions (KCl, NaCl and $CaCl_2$) at low salt concentrations ($<10^{-4}$ M) showed several orders of magnitude higher ionic conductivity compared to the bulk solution. Moreover, due to the outstanding chemical and thermal stability of BN, the ionic conduits remain fully functional at temperatures up to 90°C. The BN conduits can operate in acidic and basic environments, and do not degrade after immersing in solutions with extreme pH (pH~0 or 14) for one week. Those excellent properties make the BN ionic conduits attractive for applications in nanofluidic devices and membrane separation.

INTRODUCTION

Two-dimensional boron nitride (BN) nanosheets, the "white graphene", consist of boron and nitrogen atoms in a hexagonal plane arrangement replicating a honeycomb structure. Their properties, such as a wide band gap, thermal and chemical stability favourably differentiate them from graphene in applications when low electronic conductivity and/or enhanced environmental stability is required. However, BN nanosheet is usually hydrophobic, and thus it is difficult to form a colloidal aqueous suspension of BN nanosheets, which is required in many applications. Significant efforts have been put into isolating and functionalizing BN nanosheets to achieve better dispersion.[1-3] Recently, stable BN nanosheets colloidal suspensions were prepared by a one-step exfoliation and functionalization method based on a mechanochemical process.[4] The resulting highly water-dispersible few-layer BN further enabled the assembly of few-layer BN into free-standing membranes with lamellar microstructure.

The way ions are transported through nanoscale fluidic channels can be significantly different from that in the bulk.[5, 6] When the dimension of the fluidic channels decreases towards Debye screening length, the surface charge on the channel walls starts to play an important role in the ion transport.[7] More specifically, due to electrostatic forces, the charged channel walls attract ions of the opposite charge (counter-ions) while repelling ions of the same charge (co-ions). Thus, with an increased concentration of counter-ions and a decreased concentration of co-ions near the walls, an ionic electrical double layer forms at the channel surface.[8] Consequently, the double layer in the nanofluidic channel could effectively exclude the co-ions from the inner space of the channel. Hence, the current/conductance will be dominated by ions transport through the channel. A number of reports have demonstrated that ionic conductance in nanofluidic channel is governed by surface charges at low salt concentrations and can then be enhanced by orders of magnitude and become independent of bulk ionic concentration.[7, 9-11]

Nanofluidic processes are important in a range of applications from electrochemomechanical energy conversion[12, 13], DNA sequencing[14, 15], ionic gating[16, 17] and resistive pulse sensing[18, 19] to chemical waste decontamination and water desalination.[20-22] Various approaches, including photolithography,[7, 23] soft templating,[17, 24] and use of nanotube channels,[15, 24] have been developed to fabricate nanofluidic channels of different shapes. Meanwhile, films and membranes constructed from two-dimensional (2D) materials such as graphene oxide (GO)[25, 26] or MXene[27, 28] attract much interest. 2D nanomaterials dispersed in a solvent can easily be assembled into films or membranes by filtration. It was found that 2D capillary channels can form in GO membrane when it is hydrated.[29] Each chan-

nel formed in the GO membrane allows a monolayer of water to pass through without much impedance.[29] In addition, outstanding proton conductivity along the surface of GO[30] and a nanofluidic ion conductivity behaviour GO films[10] were reported. More recently, nano-clays were used to build 2D nanofluidic membranes.[31] The water permeable 2D capillaries formed between closely spaced 2D sheets can provide a large number of nanofluidic channels for transporting an electrolyte as well as show selectivity towards ions of different size and charge.[27] In contrast with conventional fabrication methods, building nanofluidic conduits by using membranes made of 2D materials has advantages in terms of cost, processability and feasibility. However, in highly acidic or basic conditions (pH<2 or >11), the GO membranes are nearly impermeable to water.[32] In addition, GO films may physically disintegrate in water, especially in basic solutions,[26, 33] and their quick deoxygenation happens at high pH.[34-36] Thermal deoxygenation of GO occurs at relatively low temperature.[34, 37] Therefore, extreme pH or elevated temperatures can lead to the closing of the ionic channels in GO membranes and degrade GO[34] or MXene[38]. For nanoclay, the long-term stability of the oxide membranes remains unclear, since prolonged treatment in highly acidic/basic media might result in their dissolution or damage of their structure. BN is chemically stable in acidic and basic solutions and BN membranes could be attractive and promising replacement to current 2D nanomaterial under harsh conditions. Osmotic energy conversion through ion transport has been reported on single BN nanotubes,[36] but there has been no report on the use of BN nanosheets in 2D nanofluidic applications.

Here, we report on high ionic conductivity in the nanofluidic conduits produced by BN. The BN membranes were assembled from a stable colloidal solution of BN nanosheets prepared by one-step exfoliation and functionalization.[4] Under low salt concentration, the ionic conductivity was enhanced by orders of magnitude *versus* the bulk solution. Moreover, our results also show that the BN-based nanofluidic device is highly stable and operational up to 90 °C, in highly acidic or basic solutions due to high chemical resistance and thermal stability of BN.

EXPERIMENTAL SECTION

Preparation of BN nanosheets and BN membranes. Few-layer colloidal solution of BN nanosheet was prepared as described in our previous report.[4] Briefly, h-BN (Momentive Performance Materials Inc.) and urea (Sigma-Aldrich) powders with a weight ratio of 1:20 and total weight of 10 g were milled for 20 h using a planetary ball mill (Pulverisette 7, Fritsch) at a rotation speed of 500 rpm at room temperature under nitrogen atmosphere. The milled powders were dispersed in water and dialyzed for around 1 week (membrane cutoff: 14000 kDa) in distilled water to completely remove residual urea. Stable aqueous dispersions were obtained after removing the unexfoliated BN particles via centrifugation at a low speed (RCF ~500 × g, 15 min). The white translucent and stable colloidal solution containing few-layer BN (Figure 1a) shows a highly negative zeta potential at −33.9±0.9 mV (pH ~7), in agreement with a previous work,[4] due to the B–O–H and N–O–H groups generated at the interface between h-BN and water.[4, 40] The atomic force microscopy (AFM) image and the height profile in Figure 1b show that most of the BN sheets are about 1.5 nm in thickness, corresponding to around 5 atomic layers, and have a narrow lateral size in the range of 50–100 nm.

BN membranes were assembled by vacuum filtration of the BN dispersion through an Anodisc membrane filter (25 mm diameter, 0.02 µm pore size, Whatman) similar to other 2D materials[26, 29, 41, 42]. The BN membrane can be easily peeled off from the filter after drying in air. The obtained thin membranes were white and translucent, and could be easily cut into a desired shape and size using a razor blade (Figure 1c). A typical SEM image of the cross-section of a membrane with a thickness of ~15 µm is shown in Figure 1d. The membranes used in this study have a thickness in the range of 10–25 µm. Because of the high aspect ratio of the few-layer BN nanosheets, they stacked in a well-aligned manner forming a lamellar structure, as shown in the inset of Figure 1d.

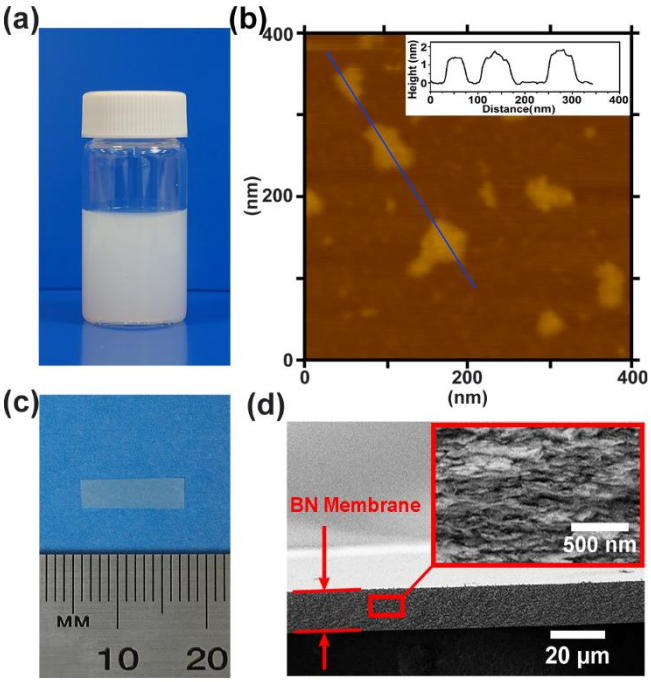

Figure 1. (a) Colloidal solution of few-layer BN, (b) AFM image of few-layer BN nanosheets on a mica substrate, inset showing corresponding height profile along the inset blue line showing thicknesses and lateral sizes of the nanosheets (c) a piece of free-standing BN membrane with size ~15 mm × 4, (d) cross-section SEM image of a BN membrane, inset showing the lamellar structure of the BN membrane constructed by few-layer BN sheets.

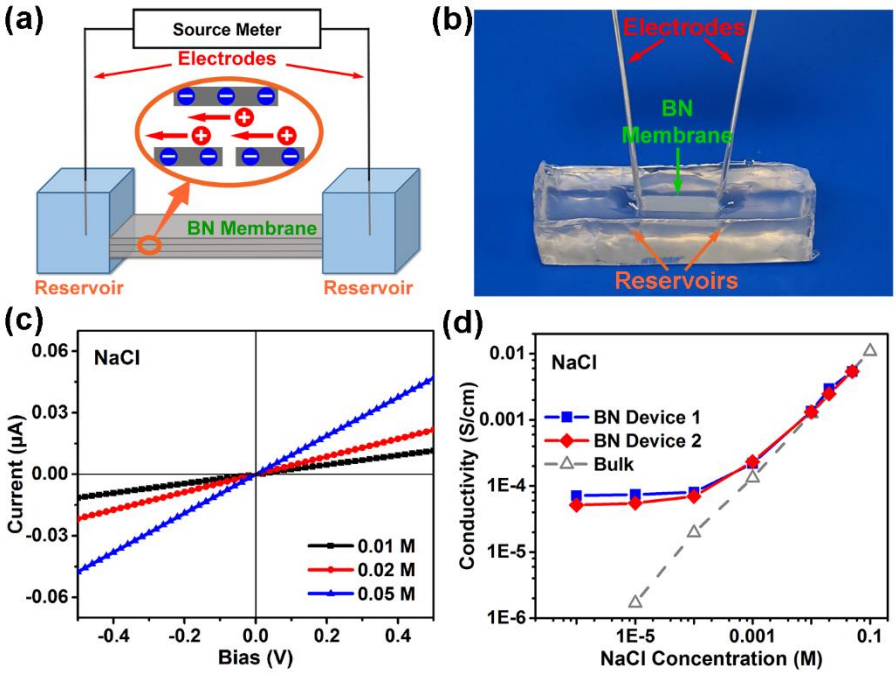

Figure 2. (a) Schematic image of the BN conduit and the testing setup, (b) photo of a BN conduit embedded in PDMS, (c) I-V curves obtained at NaCl concentrations of 0.01, 0.02, 0.05 M, (d) ionic conductivity as a function of the NaCl concentration measured on two BN conduit devices and in the bulk solution with pH ~7.

Characterization. Scanning electron microscopy (SEM) analysis was conducted using a Carl Zeiss Supra SEM. The AFM measurements were performed on a Cypher atomic force microscope. The BN solution was diluted and mildly sonicated in water, and the dispersions were dropped on a mica substrate for AFM analysis. The zeta potential of the BN colloidal solution was tested using a Malvern Zetasizer Nano ZS90. The results of zeta potential are presented as the average value of three measurements ± standard deviation. X-ray diffraction (XRD) analysis was performed with a Panalytical X'Pert Powder using a Cu Kα (λ= 1.54 Å) radiation source. Small-angle X-ray scattering (SAXS) was performed on the SAXS/WAXS beamline at the Australian Synchrotron (AS). The Pilatus-1M detector was selected for data collection and the 0.6 m camera length was selected to give a q-range of 0.05-1.6 $Å^{-1}$. The X-ray beam, of wavelength λ= 0.62 Å (20 keV) and a size of 250 μm horizontal × 150 μm vertical (FWHM), was applied to prevent the damage from long-time exposure. The exposure time was 2 s. Empty capillary or cell measurements were made and subtracted from the final data. The data were reduced by using Scattering Brain software developed at AS and FIT2D software.

Preparation and conductivity measurement of the nanofluidic conduits. The BN membranes were cut into rectangular pieces using a razor blade. The thickness of the membranes was measured by SEM analysis of the cross-section, and the average value was obtained from several measurements taken at three different locations. The rectangular BN pieces were immersed into a mixture of polydimethylsiloxane (PDMS) prepolymer and curing agent, and two reservoirs were carved in the PDMS elastomer to expose the two ends of the BN membrane as shown in Figure 1. The BN conduits device was then immersed in water for several days for fully hydrating the channels. Before each test, the device was immersed in various concentrations of electrolytes for one day to ensure that the electrolyte had fully filled the nanochannels of the conduit. To measure the ionic current, Ag/AgCl electrodes were placed into both reservoirs as source and drain. I-V curves of the BN conduits were recorded at various electrolyte concentrations from 10^{-6} M to 1 M using an IviumStat analyser. The ionic conductivity (λ) at different electrolyte concentrations across the BN conduits was calculated from the equation $\lambda = G(l/hw)$, where G is the measured conductance and l, h, and w are the length, height (thickness), and width of the channel, respectively. Length and width were taken from the measured physical dimension of the embedded conduits. The effective height h of the channels can be deduced from the conductance at high salt concentration.[10] Conductivity of the bulk solutions was tested using a TPS WP-81 conductivity meter which was calibrated before measurement. The ionic conductivity of the BN conduits was tested in different solutions with different pH. Highly purified deionized water (Milli-Q, 18 MΩ·cm) was used in all experiments.

RESULTS AND DISCUSSION

To fabricate nanofluidic conduits, BN membranes of rectangular shape (Figure 1c, d) were embedded into PDMS elastomer. Two reservoirs were carved into the PDMS to expose the two ends of the BN membrane to the electrolyte (Figure 2a, b). After soaking in deionized water for a few days to ensure full hydration of the BN membrane,

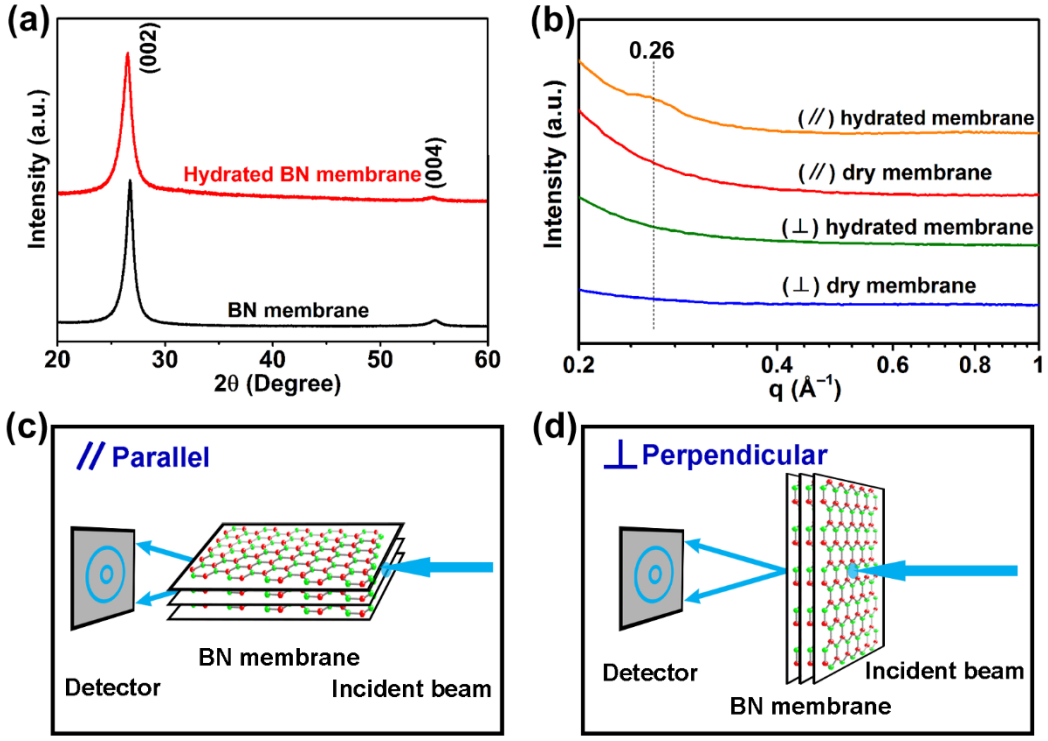

Figure 3. (a) XRD patterns of a dry BN membrane and a fully hydrated BN membrane, with (002) and (004) diffraction peaks at 26.7° and 54.9° respectively, (b) one-dimensional (1D) SAXS patterns of dry and fully hydrated BN membranes aligned perpendicular and parallel to the X-ray beam, patterns stacked by offset from the intensity scale, (c) and (d) schematics show the parallel (c) and perpendicular (d) position of the BN membrane in the SAXS analysis.

the BN conduits were immersed in the electrolyte for another day before test. The method used to test the ionic conduction in the BN conduits is schematically explained in Figure 2a. It is important to mention that the ion transport was measured along the slit channels between BN sheets, not across the sheets (Figure 2). In addition, test carried out on BN conduits before soaking (Figure S1) showed that conduits were not conductive when they were dry. Representative current-voltage (I-V) curves at various salt (NaCl) concentrations in Figure 2c show linear current response to the voltage signal. The ionic conductivity is plotted as a function of NaCl concentration in Figure 2d. As expected, the conductivity of the bulk NaCl solution without BN conduits is proportional to the NaCl concentration (straight dashed line in Figure 2d), which originates from the free migration of ions in the solution. On the other hand, the ionic conductivity of the BN conduits has two distinct characteristic behaviours at the concentrations lower and higher than 0.1 mM. At high NaCl concentration (>0.1 mM) range, the ionic conductivity is similar to that of the bulk NaCl solution, which follows a linear relationship with the concentration. On the opposite, it deviates significantly from the bulk values in the concentration range below ~0.1 mM. The conductivity then gradually approaches a plateau at lower concentrations (≤ 0.01 mM) and becomes independent of the bulk ionic concentrations. This behaviour indicates a surface-charge-governed ionic conductance at low salt concentrations.[7] Measurements on two different BN conduits with different thickness show consistent and reproducible behaviours (Figure 2d). The SEM images of two BN conduits and their corresponding IV curves are shown in Figure S2(a–d). The two conduits have a similar size ~14×6 mm (*l*×*w*). Conductance of the two conduits are shown in Figure S2 (e–f), and appear to be proportional to the thickness. Nonetheless, the conductivities of the two conduits are still highly consistent in different NaCl concentration (Figure 2d).

As different ions may behave differently when passing through a nanofluidic channel, ionic conductivity measurements were also carried out with KCl and $CaCl_2$ solutions at various concentrations. I-V curves and ionic conductivity are shown in Figure S3 as a function of electrolyte concentration. The ionic conductivity in both KCl and $CaCl_2$ electrolytes follows a trend similar to the NaCl electrolyte. At low concentrations (< 0.1 mM), the BN conduits show a greatly enhanced ionic conductivity, which is largely independent of the bulk concentration, thus representing a typical surface-charge governed ionic conductivity.

The highly negative zeta potential of the few-layer BN nanosheets suspension indicates a negative charge at the interface between BN sheets and the electrolyte.[4] To better understand the channels formation in the BN membrane, the arrangement of the BN sheets within the membrane were explored using XRD (Figure 3a) and SAXS (Figure 3b) measurements on dry and fully hydrated BN membranes. Figure 3a shows XRD patterns collected from the dry and fully hydrated BN membranes. The diffraction peaks at 26.7° and 54.9° originated from (002)

and (004) planes can be clearly seen in the hydrated BN membrane and are at almost identical positions to those of the dry BN membrane, indicating that the intrinsic structure of the few-layer BN sheets largely remains unchanged. However, the crystalline ordering of a dry membrane (FWHM=1.14º) decreases after hydration (FWHM=1.46º) from Gaussian fitting. The broader diffraction peaks in the hydrated sample are attributed to the presence of water molecules between few-layer BN sheets and therefore a less periodic spacing in *z*-direction.[27] More specifically, the (002) diffraction peaks at the same position suggest that the interlayer spacing of the BN sheets remain unchanged, which indicates that water molecules and ions did not permeate into the interlayer spacing. Therefore, the ionic conductivity of the BN conduits should be attributed only to the water molecules and ions presented in the intra-layer spacing between the BN sheets.

Figure 3b contains the one-dimensional (1D) SAXS patterns from dry and fully hydrated BN membranes aligned perpendicular and parallel to the incident beam. The patterns obtained from the membranes perpendicular to the beam are flat, indicating the absence of a distinctive structural order along the lateral direction of the membrane, similar to previous reports on GO membranes.[43] When the membranes are placed parallel to the beam, a broad X-ray scattering slope can be observed in the 1D patterns in the q<0.3 Å^{-1} vector, which could be attributed to a more uniform lamellar structure formed by stacking of BN nanosheets. A broad scatter bump in the range of 0.24–0.28 Å^{-1} and centred at 0.26 Å^{-1} is only present in the pattern recorded from the hydrated BN membrane placed parallel to the beam. It arises from the spacing between the orderly stacked and hydrated BN nanosheets. The position of this broad bump corresponds to a d spacing in the range of 22.4–26.0 Å according to the Bragg's law ($d=2\pi/q$). Taking the thickness of BN nanosheets (~5 layers, ~17 Å) into account, the actual spacing between the sheets would be within 5.4–9 Å, which accommodates 2–3 layers of water molecules.[44] This space is smaller than that estimated in the GO and graphene gel membrane.[10, 43] This space between the BN sheets allows water molecules and metal ions to pass through, and forms 2D pathways (nanochannels) for water and ions. Since the thickness of the channels is about an order of magnitude below the Debye screening length (~30 nm with monovalent ions at a concentration of 10^{-4} M), the negatively charged BN sheets efficiently attract cations (K^+, Na^+, Ca^{2+} and H^+) within an electrical double layer and repel anions (Cl^-, SO_4^{2-}, OH^-). Hence, the latter are effectively excluded from the inner space of the channels. The concentrated cations in the nanofluidic channels contribute to a higher conductivity than in the bulk solution.[7, 10, 31] Due to the small volume of the nanochannels, the double layer can easily become saturated with cations even at low concentrations. This explains the ionic conductivity plateau in the low concentration region.

It is worth mentioning that no clear dependence could be found in the conductance with respect to the pH of the electrolyte in the range of 5–9, as shown in Figure S4. In higher pH solution (pH=8–9), zeta potential is slightly more negative, which results in the slightly higher conductance. Further tests on the BN nanosheet colloidal dispersion (Figure S5) showed that in the pH range of 5–9, the zeta potential stabilized as ca. −40 mV. The variation of the zeta potential is more obvious when pH<5 or pH>9. This phenomenon is related to the protonation (low pH range)/deprotonation (high pH range) of the surface functional groups, such as amino groups and hydroxyl groups, which were introduced onto the BN nanosheets during ball-milling process.[4] Possible chemical equilibria involving two groups are:

$BN_3 + H_2O \rightleftharpoons BN_3\text{-}OH^- + H^+$

$BN_2\text{-}NH_2 + H_2O \rightleftharpoons BN_2\text{-}NH_3^+ + OH^-$

Judging from the zeta potential results, the equilibrium constants pKa for these two equilibria would be close to those from BN nanotube hydroxyl groups (pKa ~5.5)[39] and from amino groups in amino acids (pKa in the range of 9–10)[45]. Further experiments are needed to accurately determine the pKa values. The BN membranes used in this work are typically around ten to twenty micrometres in thickness and contain thousands of parallel ion channels. Therefore, the BN conduits generate higher ionic currents and have a higher surface-charge-governed conductance than the devices fabricated using conventional methods, such as lithography, which have a limited number of channels.[7, 17, 31, 46]

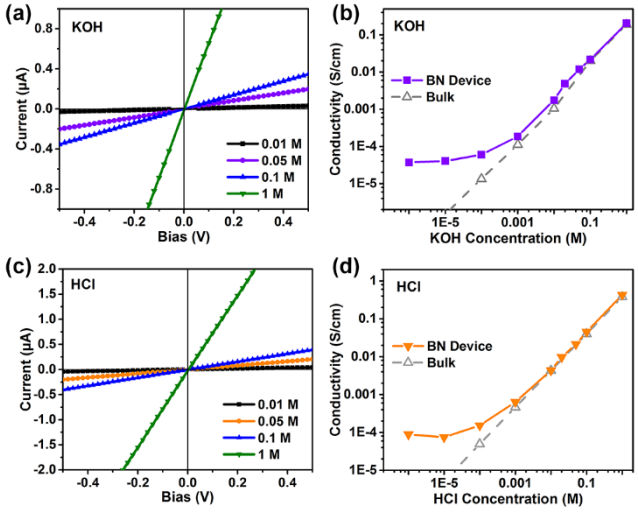

Figure 4. (a) I-V curves obtained at KOH concentrations of 0.01, 0.05, 0.1 M and 1 M (b) ionic conductivity as a function of KOH concentration, (c) I-V curves obtained at HCl concentrations of 0.01, 0.05, 0.1 M and 1 M, (d) ionic conductivity as a function of HCl concentration.

Since BN has excellent thermal and chemical stability, BN nanofluidic conduits are expected to function in highly acidic and basic solutions. Ionic conductivity tests were carried out at various HCl or KOH concentrations (up to 1 M) respectively (Figure 4). A similar surface-charge governed ionic conductivity behaviour was observed at low concentrations (generally < 0.1 mM). This experiment was repeated for five times, but the surface-charge governed

conductivity behaviour remained. For comparison purpose, we also tested the BN conduits in an acidic $NaHSO_4$ solution, and similar results were obtained (Figure S6).

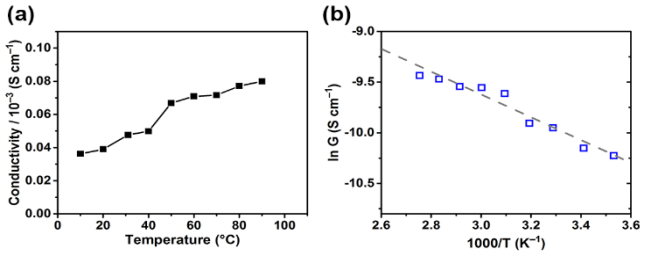

Figure 5. (a) Ionic conductivity of the BN conduits at different temperatures in 0.01 mM HCl, (b) Arrhenius plot of the conductance (ln (G)) vs. inverse temperature (1000/T) for BN conduits with 0.1 mM HCl.

After completing the routine conductivity tests with various concentrations, the BN conduits were soaked in 1 M HCl (pH ~0) and KOH (pH ~14), respectively, for an extended period up to a week. There was no visible change to the BN conduits after soaking in the solution. Conductivity test results after the extended soaking period (Figure S7), show that conductance through the BN conduits is highly stable, which further confirms that the BN membrane is able to withstand highly acidic and basic environments. The BN conduits remain fully functional in acidic and basic envirionments and even after soaking in acids and bases.

To determine the effect of temperature on the ionic conductivity and proton transport, measurements were carried out on a BN conduits devices imbued with 0.1 mM HCl with a thermometer embedded in the PDMS near the BN membrane heated in an oil bath. The conductance of the BN conduits follows an Arrhenius behaviour, as shown in Figure 5a and 5b. The activation energy is estimated to be 0.10 eV, indicating that the protons transport in the BN membrane follows a Grotthuss transport mechanism.[31, 47, 48] One of the hindrance for proton transport is solvation effects where proton interacts/bonds to the surrounding molecules or channel interior, which must be compensated to extract the proton and allow Grotthuss-like proton transport. In the BN conduits, the hydrophilic surface functional group (amino group, hydroxyl group, B–O–H and N–O–H) might play an important role in lower the barrier of proton transport and enabling the Grotthuss-like transport.[4, 48,49] It is worth mentioning that the temperature limiting factor in the aqueous electrolyte is its boiling point around 100 °C at atmospheric pressure, while the PDMS matrix can withstand temperatures up to 250 °C,[50] both of which are far below the temperature stability of BN.[51]

To estimate surface charge density, a semi-quantitative analysis of the concentration and conductivity was used.[17, 31] The ionic conductance of a single channel (G_o) was considered as the sum of two effects: the bulk ionic conductance (G_B), and the contribution of surface charges (G_S):[11]

$$G_o = G_B+G_S=(\mu_+ + \mu_-)C_BN_Aewh_o/l + 2\mu_+\sigma_s(w/l) \quad (1)$$

Here, μ_+ and μ_- are mobilities of cations and anions, respectively; C_B is the bulk salt concentration; N_A is the Avogadro's number; e is the elementary charge; w and l are the width and length of the conduits, respectively; and h_o is the height of a single nanochannel. In the case of very low concentration (strong Debye overlap), the effect of co-ions (μ_-) can be neglected. From SAXS results, h_o was estimated to be ~0.8 nm. If we consider the channels in the conduits to be an array of parallel nanoslits, we can deduce the number of channels n in a conduit from its effective height h and the d spacing from SAXS results: $n=h/d$. Therefore, the conductance of a single nanochannel is $G_o=G/n$. In KCl solution, for example, we find a surface charge density $\sigma_s \approx 0.84$ mC m^{-2}, which is much lower than that previously reported on a single BN nanotube.[39] Among the possible reasons for this discrepancy, one should note that our ball-milling process introduces surface functional groups to the BN nanosheets, especially amino groups. These species are protonated and positively charged in the pH range where the net surface charge is negative (Figure S5), so that they should partially counterbalance the high negative charge provided by "intrinsic" h-BN.[39] Besides, the estimation of the surface charge density is based on the assumption that the conduits consist of a simple array of cascading nanoslits. The evaluated surface charge depends directly on the number of channels ($G_o=G/n$) deduced from the average SAXS data. However, not all the individual BN nanosheets in the conduit may be in contact with water because of the tight stacking and random collapse in some areas. Hence, our measurement is likely overestimating the n number, thus underestimating the surface charge density. Note also that our values are comparable with those measured from 2D material membranes made of GO or vermiculite clay.[10, 31] Figure S8 shows that the predicted conductivity derived from equation (1) and the actual measured conductivity match very well. The estimated surface charge density is only a model approximation of the real membrane channel structure.

The BN conduits shown in this work are different from previously reported devices produced by conventional lithography methods,[7] based on nanotube[24], GO[10] and MXene[27, 28] membranes. The BN conduits not only generate higher ionic currents along the 2D slits and have a higher surface-charge-governed conductivity, but also remain functional in highly acidic and basic solutions. The high chemical and physical stability of BN conduits offers an opportunity for their use in a variety of applications.

CONCLUSION

Free-standing BN membranes have been assembled by filtration of few-layer BN colloidal solution and used to fabricate nanofluidic conduits that contain thousands of parallel slit-shaped ionic channels. Ionic currents have been measured through the BN nanofluidic conduits. A typical surface-charge governed conductivity, which is much higher than the bulk solution, is observed at low

salt concentrations (< 0.1 mM) of a variety of salts solution (KCl, NaCl, $CaCl_2$, HCl, NaOH and $NaHSO_4$). The BN nanofluidic conduit can withstand and remain fully functional under elevated temperatures up to 90 °C in aqueous electrolyte and extreme pH condition.

ASSOCIATED CONTENT

Supporting Information. I-V curves and conductivity measured on dry BN conduits, in KCl, $CaCl_2$, $NaHSO_4$ and Na_2SO_4; conductance measured at different pH values; ionic conductivity during soaking in 1 M KOH and 1 M HCl; and zeta potential for BN colloidal dispersion at different pH. This material is available free of charge via the Internet at http://pubs.acs.org.

AUTHOR INFORMATION

Corresponding Author

*Dr Weiwei Lei
weiwei.lei@deakin.edu.au
*Prof Ying Chen
ian.chen@deakin.edu.au

Notes

The authors declare no competing financial interest.

ACKNOWLEDGMENT

Financial support from the Australian Research Council under the Discovery program and Discovery Early Career Researcher Award are acknowledged. This research was undertaken on the SAXS/WAXS beamline (Beam time ID: M10395) at the Australian Synchrotron. Y.G. was also supported by a grant from the Qatar National Research Foundation.

REFERENCES

(1) Marsh, K. L.; Souliman, M.; Kaner, R. B. *Chem. Commun.* **2015,** *51*, 187-190.
(2) Lee, D.; Lee, B.; Park, K. H.; Ryu, H. J.; Jeon, S.; Hong, S. H. *Nano Lett.* **2015,** *15*, 1238-1244.
(3) Weng, Q.; Wang, B.; Wang, X.; Hanagata, N.; Li, X.; Liu, D.; Wang, X.; Jiang, X.; Bando, Y.; Golberg, D. *ACS Nano* **2014,** *8*, 6123-6130.
(4) Lei, W.; Mochalin, V.; Liu, D.; Qin, S.; Gogotsi, Y.; Chen, Y.*Nat. Commun.* **2015,** *6*, 8849.
(5) Sinha, S.; Pia Rossi, M.; Mattia, D.; Gogotsi, Y.; Bau, H. H. *Phys. Fluids* **2007,** *19*, 013603.
(6) Mattia, D.; Gogotsi, Y. *Microfluid. Nanofluid.* **2008,** *5*, 289-305.
(7) Stein, D.; Kruithof, M.; Dekker, C. *Phys. Rev. Lett.* **2004,** *93*, 035901.
(8) Sparreboom, W.; van den Berg, A.; Eijkel, J. C. T. *Nat. Nanotechnol.* **2009,** *4*, 713-720.
(9) Daiguji, H.; Yang, P.; Majumdar, A. *Nano Lett.* **2004,** *4*, 137-142.
(10) Raidongia, K.; Huang, J. *J. Am. Chem. Soc.* **2012,** *134*, 16528-16531.
(11) Schoch, R. B.; Renaud, P. *Appl. Phys. Lett.* **2005,** *86*, 253111.
(12) Daiguji, H.; Yang, P.; Szeri, A. J.; Majumdar, A. *Nano Lett.* **2004,** *4*, 2315-2321.
(13) Guo, W.; Cheng, C.; Wu, Y.; Jiang, Y.; Gao, J.; Li, D.; Jiang, L. *Adv. Mater.* **2013,** *25*, 6064-6068.
(14) Levy, S. L.; Craighead, H. G. *Chem. Soc. Rev.* **2010,** *39*, 1133-1152.
(15) Liu, H.; He, J.; Tang, J.; Liu, H.; Pang, P.; Cao, D.; Krstic, P.; Joseph, S.; Lindsay, S.; Nuckolls, C. *Science* **2010,** *327*, 64-67.
(16) Zhang, Z.; Kong, X.-Y.; Xiao, K.; Xie, G.; Liu, Q.; Tian, Y.; Zhang, H.; Ma, J.; Wen, L.; Jiang, L. *Adv. Mater.* **2016,** *28*, 144-150.
(17) Fan, R.; Huh, S.; Yan, R.; Arnold, J.; Yang, P. *Nat. Mater.* **2008,** *7*, 303-307.
(18) Tsutsui, M.; He, Y.; Yokota, K.; Arima, A.; Hongo, S.; Taniguchi, M.; Washio, T.; Kawai, T. *ACS Nano* **2016**, 10, 803-809.
(19) Qiu, Y.; Lin, C.-Y.; Hinkle, P.; Plett, T. S.; Yang, C.; Chacko, J. V.; Digman, M. A.; Yeh, L.-H.; Hsu, J.-P.; Siwy, Z. S. *ACS Nano* **2016**, 10, 8413-8422.
(20) Humplik, T.; Lee, J.; O'Hern, S. C.; Fellman, B. A.; Baig, M. A.; Hassan, S. F.; Atieh, M. A.; Rahman, F.; Laoui, T.; Karnik, R.; Wang, E. N. *Nanotechnology* **2011**, 22, 292001.
(21) Kim, S. J.; Ko, S. H.; Kang, K. H.; Han, J. *Nat. Nano.* **2010**, 5, 297-301.
(22) Shannon, M. A.; Bohn, P. W.; Elimelech, M.; Georgiadis, J. G.; Marinas, B. J.; Mayes, A. M. *Nature* **2008**, 452, 301-310.
(23) Kim, S. J.; Wang, Y.-C.; Lee, J. H.; Jang, H.; Han, J. *Phys. Rev. Lett.* **2007,** *99*, 044501.
(24) Goldberger, J.; Fan, R.; Yang, P. *Acc. Chem. Res.* **2006,** *39*, 239-248.
(25) Hu, S.; Lozada-Hidalgo, M.; Wang, F. C.; Mishchenko, A.; Schedin, F.; Nair, R. R.; Hill, E. W.; Boukhvalov, D. W.; Katsnelson, M. I.; Dryfe, R. A. W.; Grigorieva, I. V.; Wu, H. A.; Geim, A. K. *Nature* **2014,** *516*, 227-30.
(26) Yeh, C.-N.; Raidongia, K.; Shao, J.; Yang, Q.-H.; Huang, J. *Nature Chem.* **2015,** *7*, 166-170.
(27) Ren, C. E.; Hatzell, K. B.; Alhabeb, M.; Ling, Z.; Mahmoud, K. A.; Gogotsi, Y. *J. Phys. Chem. Lett.* **2015,** *6*, 4026-4031.
(28) Ghidiu, M.; Halim, J.; Kota, S.; Bish, D.; Gogotsi, Y.; Barsoum, M. W. *Chem. Mater.* **2016,** *28*, 3507-3514.
(29) Nair, R. R.; Wu, H. A.; Jayaram, P. N.; Grigorieva, I. V.; Geim, A. K. *Science* **2012,** *335*, 442-444.
(30) Karim, M. R.; Hatakeyama, K.; Matsui, T.; Takehira, H.; Taniguchi, T.; Koinuma, M.; Matsumoto, Y.; Akutagawa, T.; Nakamura, T.; Noro, S.-i.; Yamada, T.; Kitagawa, H.; Hayami, S. *J. Am. Chem. Soc.* **2013,** *135*, 8097-8100.
(31) Shao, J.-J.; Raidongia, K.; Koltonow, A. R.; Huang, J. *Nat. Commun.* **2015,** *6*, 7602.
(32) Huang, H.; Mao, Y.; Ying, Y.; Liu, Y.; Sun, L.; Peng, X. *Chem. Commun.* **2013,** *49*, 5963-5965.
(33) Sun, P.; Zhu, M.; Wang, K.; Zhong, M.; Wei, J.; Wu, D.; Xu, Z.; Zhu, H. *ACS Nano* **2013,** *7*, 428-437.
(34) Kar, T.; Devivaraprasad, R.; Singh, R. K.; Bera, B.; Neergat, M. *RSC Adv.* **2014,** *4*, 57781-57790.
(35) Fan, X.; Peng, W.; Li, Y.; Li, X.; Wang, S.; Zhang, G.; Zhang, F. *Adv. Mater.* **2008,** *20*, 4490-4493.
(36) Rourke, J. P.; Pandey, P. A.; Moore, J. J.; Bates, M.; Kinloch, I. A.; Young, R. J.; Wilson, N. R. *Angew. Chem. Int. Ed.* **2011,** *50*, 3173-3177.
(37) Eigler, S.; Grimm, S.; Hirsch, A. *Chem. Eur. J.* **2014,** *20*, 984-989.
(38) Ahmed, B.; Anjum, D. H.; Hedhili, M. N.; Gogotsi, Y.; Alshareef, H. N. *Nanoscale* **2016,** *8*, 7580-7587.
(39) Siria, A.; Poncharal, P.; Biance, A.-L.; Fulcrand, R.; Blase, X.; Purcell, S. T.; Bocquet, L. *Nature* **2013**, 494, 455-458.
(40) Crimp, M. J.; Oppermann, D. A.; Krehbiel, K. *J. Mater. Sci.* **1999,** *34*, 2621-2625.
(41) Liu, D.; He, L.; Lei, W.; Klika, K. D.; Kong, L.; Chen, Y. *Adv. Mater. Interfaces* **2015,** *2*, 1500228.

(42) Huang, L.; Zhang, M.; Li, C.; Shi, G. *J. Phys. Chem. Lett.* **2015,** *6*, 2806-2815.
(43) Cheng, C.; Jiang, G.; Garvey, C. J.; Wang, Y.; Simon, G. P.; Liu, J. Z.; Li, D. *Science Advances* **2016,** *2*, e1501272.
(44) Tansel, B.; Sager, J.; Rector, T.; Garland, J.; Strayer, R. F.; Levine, L.; Roberts, M.; Hummerick, M.; Bauer, J. *Sep. Purif. Technol.* **2006,** *51*, 40-47.
(45) Carey, F. A., *Organic Chemistry*. 4 ed.; McGraw-Hill Education: 2000.
(46) Duan, C.; Majumdar, A. *Nat. Nanotechnol.* **2010,** *5*, 848-852.
(47) Agmon, N. *Chem. Phys. Lett.* **1995,** *244*, 456-462.
(48) Tunuguntla, R. H.; Allen, F. I.; Kim, K.; Belliveau, A.; Noy, A. *Nat. Nanotechnol.* **2016,** *11*, 639-44.
(49) Dellago, C.; Hummer, G. *Phys. Rev. Lett.* **2006**, 97, 245901
(50) Radhakrishnan, T. S. *J. Appl. Polym. Sci.* **2006,** *99*, 2679-2686.
(51) Kostoglou, N.; Polychronopoulou, K.; Rebholz, C. *Vacuum* **2015,** *112*, 42-45.

Insert Table of Contents artwork here